PHYSICAL REVIEW B VOLUME 52, NUMBER 5 1 AUGUST 1995-I

Symmetries and mean-field phases of the extended Hubbard model

Anders B. Eriksson,* Torbjörn Einarsson, and Stellan Östlund
Institute of Theoretical Physics, Chalmers University of Technology and Gothenburg University, S-41296 Göteborg, Sweden

(Received 21 November 1994; revised manuscript received 3 March 1995)

The two-dimensional extended Hubbard model that includes a nearest-neighbor Heisenberg interaction is studied using a mean-field theory where quasiparticles are defined by an U(8) group of canonical transformations permitting both broken gauge, spin, and sublattice symmetry. The theory is further extended to incorporate a possible twist in the spin-quantization axis, so that the competition between superconductivity, charge-density waves, and Néel and spiral antiferromagnetic order can be monitored within one single theory. Our results for positive Hubbard U and Heisenberg exchange J suggest that antiferromagnetic ordering dominates close to half-filling, while spiral states and d-wave superconductivity compete when doping is introduced. For moderate values of J, we find a phase diagram where a phase transition occurs from an antiferromagnet to a d-wave superconductor as doping is increased. A narrow region of $(s + id)$-wave superconductor is found for some values of J and U.

I. INTRODUCTION

For many years the two-dimensional (2D) Hubbard and "extended" Hubbard model have served as simple models of high-T_c materials and a paradigm of strongly correlated electrons. However, despite many creative attempts to develop approximations to attack the problem, the 2D Hubbard model has defied a definitive analysis.

In contrast to many of those efforts, the goal in the present paper is not to try to model the behavior of high-T_c superconductors or even to make particularly strong statements about the 2D Hubbard model. Rather, we wish to make a definitive analysis of the BCS mean-field theory, an approximation method that has been remarkably successful in gaining information about simpler model systems with both broken spin and gauge symmetry. It is clearly important that we know what this simple approximation has to say about the Hubbard model before we can be confident in applying more sophisticated techniques.

Although the program sounds straightforward, the method becomes surprisingly complicated if one insists on preserving the symmetries known to exist in the Hubbard model at half-filling. The complication is due to the exact $\mathrm{SO}(4) \approx \mathrm{SU}(2) \times \mathrm{SU}(2)$ symmetry[1] precisely at half-filling and that this symmetry mixes many phases that are typically ignored in simpler calculations. To do a proper job, we must therefore include all the order parameters that have been discussed before for this system, among them spiral spin waves,[2–6] Néel antiferromagnetism,[7–9] d-wave and s-wave superconductivity,[7,10–13] as well as all other phases that are related to these via the symmetry group.[14,8]

A consequence is that a multitude of possible order parameters must be retained to provide a self-consistent theory. Our mean-field theory systematically enumerates a very large set of representations of the possible broken symmetries and, among other phases, allows for the possibility of all types of ordered phases that have been discussed in previous analyses, including antiferromagnetism, spiral spin waves, and d-wave superconductivity.

The mean-field theory that we employ is based on a U(8) set of canonical transformations yielding a united treatment of superconductivity,[15–17] charge-density waves, and spin-density waves[18] as was first demonstrated by Solomon and Birman[19] in 1987. The theory is analogous to the use of U(2) transformations in the analysis of broken gauge symmetry in BCS theory.[15,16]

The organization of the rest of this paper is the following: after providing a brief review of related results in Sec. II, we analyze the symmetry of the Hubbard model in Sec. III. The representations of the $\mathrm{SU}(2)\times\mathrm{SU}(2)$ symmetry group is made via an 8×8 Clifford algebra, which provides a generalization of the Dirac and Pauli matrices used previously in the Nambu formalism applied in the study of BCS theory and $^3\mathrm{He}$.[20] In Sec. IV, we derive the mean-field theory for the Hubbard model at half-filling and introduce the point-group symmetry, while in Sec. V we extend the analysis to include the possibility of spiral antiferromagnetic states that have been proposed as likely phases away from half-filling. We discuss the reformulation of the self-consistent equations in Sec. VI, and the numerical solution procedure in Sec. VII. Our results are presented in the form of phase diagrams in Sec. VIII, before the final discussion in Sec. IX. Appendixes provide additional mathematical details.

II. BACKGROUND

The Hubbard model is given by the Hamiltonian

$$H = H_0 - \mu \hat{N} + H_{\mathrm{Hubb}} , \tag{1}$$

where

$$H_0 = -t \sum_{\langle \mathbf{R},\mathbf{R}' \rangle,\sigma} (c^\dagger_{\mathbf{R},\sigma} c_{\mathbf{R}',\sigma} + \mathrm{H.c.}) , \tag{2}$$

0163-1829/95/52(5)/3662(14)/$06.00

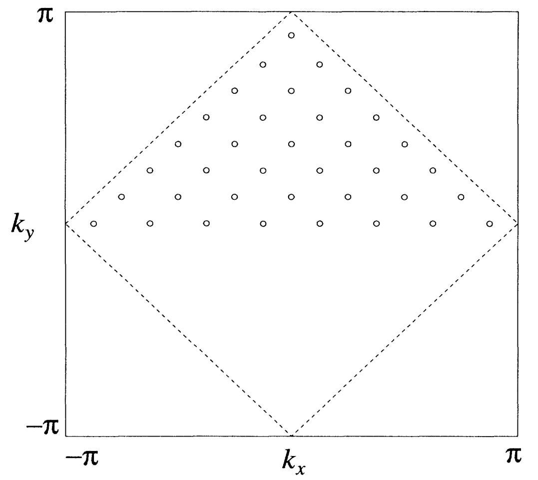

FIG. 1. The first Brillouin zone of the square lattice with lattice constant 1. The line $\epsilon_{\mathbf{k}} = 0$ is indicated as well as the $\mathbf{k}$ points in the reduced zone that are used in a numerical simulation with 32 $\mathbf{k}$ points (Sec. VII). The contributions from the points on the k_x axes are scaled down by a factor of 2 since they would otherwise be overcounted.

where the summation denoted by $\sum''$ runs over the four times *reduced* Brillouin zone corresponding to $\epsilon_{\mathbf{k}} < 0$ and $k_y \geq 0$ (see Fig. 1). Note the special order of the operators in Eq. (8).

We next introduce the "Shiba" transformation Z which acts on the *position space* creation and destruction operators $c^\dagger_{\mathbf{r},\sigma}$ through the canonical transformation $c^\dagger_{\mathbf{r},\downarrow} \mapsto (-1)^{\mathbf{r}} c_{\mathbf{r},\downarrow}$, $c^\dagger_{\mathbf{r},\uparrow} \mapsto c^\dagger_{\mathbf{r},\uparrow}$, where the factor $(-1)^{\mathbf{r}} \equiv e^{i\mathbf{Q}\cdot\mathbf{r}}$ induces a change of sign on one sublattice. The Shiba transformation is hence a particle-hole transformation, together with a local change of gauge, which only acts on the spin-down operators.

In reciprocal space, spin rotations and Z act naturally on the eight-component multispinor $\Psi_{\mathbf{k}} \equiv (a_{\mathbf{k},\uparrow}, a_{\mathbf{k},\downarrow}, b_{\mathbf{k},\uparrow}, b_{\mathbf{k},\downarrow}, a^\dagger_{-\mathbf{k},\uparrow}, a^\dagger_{-\mathbf{k},\downarrow}, b^\dagger_{-\mathbf{k},\uparrow}, b^\dagger_{-\mathbf{k},\downarrow})$ which carries definite momentum $\mathbf{k}$ mod $\mathbf{Q}$. In this basis, Z is represented by an idempotent matrix whose entries are all zero except $Z_{1,1} = Z_{3,3} = Z_{5,5} = Z_{7,7} = Z_{2,8} = Z_{4,6} = Z_{6,4} = Z_{8,2} = 1$, and which acts on $\Psi_{\mathbf{k}}$ by matrix-vector multiplication, $\Psi_{\mathbf{k}} \mapsto \Psi_{\mathbf{k}} Z$. It is well known that Z is an exact symmetry of H_0 but changes the sign of the Hubbard term U.[29,31–34] It is also simple to verify that the nearest-neighbor Heisenberg term H_{Heis} is invariant under Z.

A pseudospin transformation R' is defined as $R' = ZRZ$ where R is an ordinary global SU(2) spin rotation. Since $[H,Z] = 0$ and $[H,R] = 0$, we have $[H,R'] = 0$, and since Z does not commute with R, we see that the entire symmetry group of H is $\mathcal{S} = \text{SU}(2) \times \text{SU}(2)$. It follows further that because $\Psi_{\mathbf{k}}$ defines a representation of both R and Z, it also determines a representation of $\mathcal{S}$.

B. A basis spanning the space of Hermitian 8 × 8 matrices

To represent the action of spin and pseudospin transformations on the basis $\Psi_{\mathbf{k}}$, we introduce a set of seven Hermitian 8×8 matrices β_A constructed in blocks from the ordinary Dirac matrices γ_ν as shown in Table I. By explicit computation, it can be verified that β_A form a Clifford algebra,[35] i.e., $\beta_A\beta_B + \beta_B\beta_A = 2g_{AB}$, where $g_{AB} = 0$ except for $g_{00} = \mathbb{1}$ and $g_{nn} = -\mathbb{1}$, $n = 1,\ldots,6$.

The β_A matrices have been constructed so that $(\beta_1,\beta_2,\beta_3)$ transform as a vector under spin rotations and $(\beta_4,\beta_5,\beta_6)$ transform as a vector under pseudospin rotations, while $(\beta_4,\beta_5,\beta_6)$ and $(\beta_1,\beta_2,\beta_3)$ transform as a scalar under spin and pseudospin rotations, respectively. Taking multiple products of the matrices β_A, one can construct a complete basis for the vector space of 8×8 Hermitian matrices (with real-valued coefficients). The Clifford algebra contains four independent spin/pseudospin scalars, and it follows that there are also four independent sets of spin and pseudospin vectors and spin⊗pseudospin tensors, making a total of $4 \times (1 + 3 + 3 + 9) = 64$ basis elements which together span the space of 8×8 Hermitian matrices.[30]

Our goal is to construct a basis that has simple transformation properties under spin and pseudospin rotations, and with the above classification scheme in mind, we label the 64 base matrices by $B^\kappa_{\mu\nu}$, where $0 \leq \mu,\nu,\kappa \leq 3$. The upper index κ enumerates each of the four independent sets of matrices associated with each of the four scalars. Transformation properties under spin rotations are indexed by μ, where scalars carry the index $\mu = 0$, while $\mu = 1,2,3$ represents the components of a spin vector. Similarly ν identifies pseudospin scalars and vectors. For example, B^2_{01} transforms as a scalar under spin rotations and as the first component of a pseudospin vector. The matrices $B^\kappa_{\mu\nu}$ are constructed so that they are not only Hermitian, but also have natural transformation properties under parity, sublattice exchange, and time reversal, and so that the indices μ and ν are simply interchanged under Z.

To explicitly construct the basis matrices we introduce the four scalars. Three of them are the identity matrix $\mathbb{1}$, β_0, and $\Gamma = i\beta_0\beta_1\beta_2\beta_3 = \left(\begin{smallmatrix}\gamma_5 & 0\\ 0 & \gamma_5\end{smallmatrix}\right)$, where γ_5 indicates the

TABLE I. Construction of the 8×8 β_A matrices from the 4×4 Dirac matrices expressed in terms of Pauli matrices. The index j runs from 1 to 3. The notation γ_j^* denotes complex conjugate (*not adjoint*).

Pauli	$(\sigma_1,\sigma_2,\sigma_3) = \left[\begin{pmatrix}0 & 1\\ 1 & 0\end{pmatrix}, \begin{pmatrix}0 & -i\\ i & 0\end{pmatrix}, \begin{pmatrix}1 & 0\\ 0 & -1\end{pmatrix}\right]$
4×4 Dirac	$\gamma_0 = \begin{pmatrix}\mathbb{1} & 0\\ 0 & -\mathbb{1}\end{pmatrix}$ $\gamma_j = \begin{pmatrix}0 & \sigma_j\\ -\sigma_j & 0\end{pmatrix}$
8×8 β_A	$\beta_0 = \begin{pmatrix}\gamma_0 & 0\\ 0 & -\gamma_0\end{pmatrix}$ $\beta_j = \begin{pmatrix}\gamma_j & 0\\ 0 & \gamma_j^*\end{pmatrix}$
	$\beta_{j+3} = iZ\beta_0\beta_j Z$

the Hamiltonian *before* the mean-field approximation is applied.

To describe any spiral we need a 2D vector $\mathbf{q}$ in the plane, which controls the direction and pitch of the spiral spin wave, and a 3D unit vector $\boldsymbol{\Omega}$ which defines the axis around which the spin is twisted. The spin-twisting canonical transformation is then generated by the operator

$$\begin{pmatrix} c^\dagger_{\mathbf{r},\uparrow} & c^\dagger_{\mathbf{r},\downarrow} \end{pmatrix} \exp[i(\mathbf{q}\cdot\mathbf{r})(\boldsymbol{\Omega}\cdot\boldsymbol{\sigma})] \begin{pmatrix} c_{\mathbf{r},\uparrow} \\ c_{\mathbf{r},\downarrow} \end{pmatrix} , \qquad (21)$$

where $\boldsymbol{\sigma}$ is the vector of Pauli matrices. This canonical transformation is easily written as a unitary transformation of the creation/annihilation operators,

$$\begin{pmatrix} c^\dagger_{\mathbf{r},\uparrow} \\ c^\dagger_{\mathbf{r},\downarrow} \end{pmatrix} \to [\cos(\mathbf{q}\cdot\mathbf{r})\mathbb{1} + i\sin(\mathbf{q}\cdot\mathbf{r})\boldsymbol{\Omega}\cdot\boldsymbol{\sigma}] \begin{pmatrix} c^\dagger_{\mathbf{r},\uparrow} \\ c^\dagger_{\mathbf{r},\downarrow} \end{pmatrix} . \qquad (22)$$

Since the Hamiltonian is invariant under global spin rotations the direction of $\boldsymbol{\Omega}$ can be arbitrarily set to be along $\hat{z}$.

When applying this spiral spin transformation to H, the Hubbard interaction is invariant since it is spin-rotation invariant and on site, but the hopping term transforms into $H_0^{\mathbf{q}} = \sum_{\mathbf{k}} \epsilon_{\mathbf{k}}(n_{\mathbf{k}+\mathbf{q},\uparrow} + n_{\mathbf{k}-\mathbf{q},\downarrow})$, which, using our operator definitions, is written as

$$\langle H_0^q \rangle = -2t \sum_{\mathbf{k},n=x,y}{}'' 8[\cos(q_n)\cos(k_n)\langle(\alpha^1_{00})_{\mathbf{k}}\rangle + \sin(q_n)\sin(k_n)\langle(\alpha^0_{30})_{\mathbf{k}}\rangle] . \qquad (23)$$

The Heisenberg term transforms into $H^{\mathbf{q}}_{\mathrm{Heis}} = J\sum_{\langle\mathbf{R},\mathbf{R}'\rangle} \vec{S}_{\mathbf{R}}\cdot\vec{S}_{\mathbf{R}'}\cos[2\mathbf{q}\cdot(\mathbf{R}-\mathbf{R}')] + 2S^z_{\mathbf{R}}S^z_{\mathbf{R}'}\sin^2[\mathbf{q}\cdot(\mathbf{R}-\mathbf{R}')]$, where $S^z_{\mathbf{R}}$ denotes the z component of the local spin operator at site $\mathbf{R}$. Using the same notation as in Eqs. (18) and (19) with the extension that ι is an index that is summed over 1 and 2 only, the Heisenberg expectation value is

$$\begin{aligned} \langle H^{\mathbf{q}}_{\mathrm{Heis}}\rangle = \frac{16J}{N} \sum_{\substack{\mathbf{k},\mathbf{k}' \\ n=x,y}}{}'' \Bigg[& \langle\alpha^1_{30}\rangle^2_{\mathbf{k}\mathbf{k}'} - \langle\alpha^3_{30}\rangle^2_{\mathbf{k}\mathbf{k}'} + \cos(q_n)[\langle\alpha^1_{\iota 0}\rangle^2_{\mathbf{k}\mathbf{k}'} - \langle\alpha^3_{\iota 0}\rangle^2_{\mathbf{k}\mathbf{k}'}] + \frac{1}{2}\cos(k_n)\cos(k'_n) \\ & \times\Big\{ -[1+2\cos(2q_n)][\langle\alpha^1_{00}\rangle^2_{\mathbf{k}\mathbf{k}'} + \langle\alpha^2_{0i}\rangle^2_{\mathbf{k}\mathbf{k}'}] + \langle\alpha^2_{\iota 0}\rangle^2_{\mathbf{k}\mathbf{k}'} + \langle\alpha^1_{\iota i}\rangle^2_{\mathbf{k}\mathbf{k}'} + [2\cos(2q_n)-1][\langle\alpha^2_{30}\rangle^2_{\mathbf{k}\mathbf{k}'} + \langle\alpha^1_{3i}\rangle^2_{\mathbf{k}\mathbf{k}'}] \Big\} \\ & + \sin(k_n)\sin(k'_n)\Big\{ -[1+2\cos(2q_n)][\langle\alpha^3_{00}\rangle^2_{\mathbf{k}\mathbf{k}'} + \langle\alpha^0_{0i}\rangle^2_{\mathbf{k}\mathbf{k}'}] + \langle\alpha^0_{\iota 0}\rangle^2_{\mathbf{k}\mathbf{k}'} + \langle\alpha^3_{\iota i}\rangle^2_{\mathbf{k}\mathbf{k}'} \\ & + [2\cos(2q_n)-1][\langle\alpha^0_{30}\rangle^2_{\mathbf{k}\mathbf{k}'} + \langle\alpha^3_{3i}\rangle^2_{\mathbf{k}\mathbf{k}'}] \Big\} \Bigg] . \end{aligned} \qquad (24)$$

The large number of terms in this expression is due to the broken spin-rotational and point-group symmetries.

VI. SOLVING FOR THE STATE OF LOWEST FREE ENERGY

A. Self-consistent equations at finite temperature

In the spirit of standard BCS theory we introduce the reduced Hamiltonian

$$H = \sum_{l,m,\mathbf{k}}{}'' a_{l,m}\beta^l_{\mathbf{k}}\alpha^m_{\mathbf{k}} + \sum_{l,m,\mathbf{k},\mathbf{k}'}{}'' b_{l,m}\beta^l_{\mathbf{k}}\beta^l_{\mathbf{k}'}\alpha^m_{\mathbf{k}}\alpha^m_{\mathbf{k}'} , \qquad (25)$$

which has the generic expectation value given in Eq. (20). We also define the mean-field order parameters (gap functions)

$$\Delta_{l,m} = \sum_{\mathbf{k}}{}'' \beta^l_{\mathbf{k}}\langle\alpha^m_{\mathbf{k}}\rangle . \qquad (26)$$

Using the assumption that the fluctuations in the operators $\alpha^m_{\mathbf{k}}$ from their mean-field values are small, we substitute $\alpha^m_{\mathbf{k}} = (\alpha^m_{\mathbf{k}} - \langle\alpha^m_{\mathbf{k}}\rangle) + \langle\alpha^m_{\mathbf{k}}\rangle$ into H in Eq. (25), drop terms quadratic in $(\alpha^m_{\mathbf{k}} - \langle\alpha^m_{\mathbf{k}}\rangle)$, and find the mean-field Hamiltonian H_{mf},

$$H_{\mathrm{mf}} = \sum_{l,m,\mathbf{k}}{}'' (a_{l,m} + 2b_{l,m}\Delta_{l,m})\beta^l_{\mathbf{k}}\alpha^m_{\mathbf{k}} - \sum_{l,m}\Delta^2_{l,m} . \qquad (27)$$

Aside from a constant that is unimportant in this discussion, H_{mf} can be recast in the form

$$H_{\mathrm{mf}} = \tfrac{1}{8}\sum_{\mathbf{k}}{}'' \mathrm{Tr}[h(\mathbf{k})(\Psi^\dagger_{\mathbf{k}} \otimes \Psi_{\mathbf{k}})], \qquad (28)$$

where

$$h(\mathbf{k}) = \sum_{l,m}(a_{l,m} + 2b_{l,m}\Delta_{l,m})\beta^l_{\mathbf{k}}B_m . \qquad (29)$$

Introducing the matrix of expectation values $f_{\mathbf{k}} \equiv \langle(\Psi^\dagger_{\mathbf{k}} \otimes \Psi_{\mathbf{k}})\rangle$, it follows from Eqs. (16) and (26) that

$$\Delta_{l,m} = \tfrac{1}{8}\sum_{\mathbf{k}}{}'' \beta^l_{\mathbf{k}}\mathrm{Tr}\,(B_m f_{\mathbf{k}}) . \qquad (30)$$

To evaluate $f_{\mathbf{k}}$ we note that the mean-field Hamiltonian is bilinear in $\Psi^\dagger_{\mathbf{k}}$ and can be diagonalized, $H_{\mathrm{mf}} = \sum''_{\alpha,\mathbf{k}} \epsilon_\alpha(\mathbf{k})(\chi^\dagger_{\mathbf{k}})^\alpha(\chi_{\mathbf{k}})^\alpha$, by the canonical transformation $\chi^\dagger_{\mathbf{k}} = U_{\mathbf{k}}\Psi^\dagger_{\mathbf{k}}$, where $U_{\mathbf{k}}$ is an U(8) matrix. Standard arguments from statistical mechanics give in the diagonal case

$$\langle(\chi_{\mathbf{k}}^{\dagger}\otimes\chi_{\mathbf{k}})_{\alpha,\gamma}\rangle=(1+e^{\beta\epsilon_{\alpha}(\mathbf{k})})^{-1}\delta_{\alpha\gamma} \tag{31}$$

(β is the inverse temperature, $\beta=1/k_BT$) which, when transformed back to the operators $\Psi_{\mathbf{k}}$, results in

$$f_{\mathbf{k}}=\langle(\Psi_{\mathbf{k}}^{\dagger}\otimes\Psi_{\mathbf{k}})\rangle=(1+e^{\beta h(\mathbf{k})})^{-1}\,. \tag{32}$$

Equations (29), (30), and (32) constitute the self-consistent equations to be solved for $\Delta_{l,m}$. The solutions extremize the free energy F,

$$F=\langle H\rangle-TS\,, \tag{33}$$

where $\langle H\rangle$ now includes the chemical potential, and where S is the entropy. If more than one solution is found, then the one with the minimal value of F is the physical one. To calculate F, both terms in Eq. (33) must be explicitly evaluated. The evaluation of $\langle H\rangle$ is straightforward—using Eq. (20) we see that it is equal to

$$\langle H\rangle=\sum_{l,m}(a_{l,m}\Delta_{l,m}+b_{l,m}\Delta_{l,m}^{2})\,. \tag{34}$$

The entropy is in turn given by

$$S=-k_B{\sum_{\mathbf{k}}}''\mathrm{Tr}[f_{\mathbf{k}}\ln f_{\mathbf{k}}+(1-f_{\mathbf{k}})\ln(1-f_{\mathbf{k}})]\,, \tag{35}$$

where $f_{\mathbf{k}}$ is the matrix of expectation values defined in Eq. (32).

B. Zero temperature

At zero temperature, the variational state gives an approximate ground state $|G\rangle$ and the thermal expectation values evolve into expectation values with respect to this ground state, i.e., $\langle(\Psi_{\mathbf{k}}^{\dagger}\otimes\Psi_{\mathbf{k}})\rangle$ is replaced by $\langle G|\Psi_{\mathbf{k}}^{\dagger}\otimes\Psi_{\mathbf{k}}|G\rangle$. The zero-temperature self-consistent equations are obtained from Eq. (30) in the limit $\beta\to\infty$.

Combining the facts that the ground state is the vacuum state for the quasiparticles and that the first (last) four elements of $\chi_{\mathbf{k}}$ are annihilation (creation) operators, we can identify the diagonal matrix $g=\langle G|(\chi_{\mathbf{k}}^{\dagger}\otimes\chi_{\mathbf{k}})|G\rangle$. Its diagonal entries are $(0,0,0,0,1,1,1,1)$, and from Eq. (31) with $\beta\to\infty$ it follows that four of the eigenvalues of $h(\mathbf{k})$ must be negative and the rest positive. We then solve for the unitary matrices $U_{\mathbf{k}}$ that diagonalize the $h(\mathbf{k})$'s defined in Eq. (29), in such a way that the eigenvalues in the diagonal matrices $D_{\mathbf{k}}$ are in descending order. The self-consistent equations to be iterated are then Eq. (29) and

$$\Delta_m=\frac{1}{8}{\sum_{\mathbf{k}}}''\beta_{\mathbf{k}}^{m}\,\mathrm{Tr}(B_mU_{\mathbf{k}}^{\dagger}gU_{\mathbf{k}})\,, \tag{36a}$$

$$D_{\mathbf{k}}=U_{\mathbf{k}}h(\mathbf{k})U_{\mathbf{k}}^{\dagger}\,. \tag{36b}$$

C. An alternative set of equations for the ground state at half-filling

The self-consistent equations must be solved numerically. Although the equations are formally simple, it is quite challenging to numerically carry out a search of the solution space. We therefore present an alternative method to find the ground state, and use it to derive a theorem of stability of the superconducting and the antiferromagnetic solutions at half-filling for some regimes of U and J.

Naïvely, the expectation value of the Hamiltonian, Eq. (20), is a simple quadratic form and one should just find its minimum. However, since the expectation values $\langle\alpha_{\mathbf{k}}^{m}\rangle$ are constrained by the fact that they represent expectation values of fermion operators, the terms cannot be independently varied, and there are constraints on the set of $\langle\alpha_{\mathbf{k}}^{m}\rangle$. These restrictions were automatically satisfied in the previous analysis, since $\alpha_{\mathbf{k}}^{m}$ was explicitly computed through a canonical transformation. Another way to proceed is to try to find a constrained quadratic minimum directly without first calculating a canonical transformation.

To express the fermionic constraints, we define the following matrix:

$$A_{\mathbf{k}}=\sum_{\substack{m\neq m'\\ m,m'\neq 0}}\langle\alpha_{\mathbf{k}}^{m}\rangle\langle\alpha_{\mathbf{k}}^{m'}\rangle\{B_m,B_{m'}\}\,, \tag{37}$$

where $\{A,B\}$ denotes the anticommutator $\{A,B\}\equiv AB+BA$. The matrix $B_0\equiv B_{00}^{0}=-\mathbb{1}$ that is excluded from the sum is the only basis matrix with nonzero trace. First we state the lemma that reformulates the problem of minimizing the energy.

Lemma 1. *The restrictions on the expectation values* $\langle\alpha_{\mathbf{k}}^{m}\rangle$ *for the variational solutions of Eq. (20) are* $\sum_m\langle\alpha_{\mathbf{k}}^{m}\rangle^2=\frac{1}{2}$, $\langle(\alpha_{00}^{0})_{\mathbf{k}}\rangle=-\frac{1}{2}$, *and* $A_{\mathbf{k}}=0\;\forall\,\mathbf{k}$.

This lemma is proved in Appendix B. The importance of the lemma is that it shows that the minimization problem of Eq. (20) is a quadratic minimum subject to quadratic constraints. This enables us to search for minima of the *unconstrained* problem, which, if they are found to satisfy the constraints, must also be minima of the constrained problem. A class of such solutions are introduced in the following theorem (proved in Appendix B) and corollary.

Theorem 1. *Consider the Hamiltonian in Eq. (20) with fixed coefficients* $a_{l,m}$ *and* $b_{l,m}$. *Define* $\mathcal{N}$ *as the subset of purely quadratic and irreducible terms,* $\mathcal{N}=\{m:a_{l,m}=0\,\forall\,l\;,b_{l,m}=b_m\delta_{l,l(m)}\}$, *where* $l(m)$ *is a function which attaches one single* l *to each* m. *Assume there exists an* $\tilde{m}\in\mathcal{N}$, *such that* ($b_{\tilde{m}}<0$ *and* $b_{\tilde{m}}|\beta_{\mathbf{k}}^{l(\tilde{m})}\beta_{\mathbf{k}'}^{l(\tilde{m})}|<b_m|\beta_{\mathbf{k}}^{l(m)}\beta_{\mathbf{k}'}^{l(m)}|\,\forall\,\mathbf{k},\mathbf{k}',\,\forall\,m\in\mathcal{N}\setminus\{\tilde{m}\}$). *If* ($\langle\alpha_{\mathbf{k}}^{m}\rangle=0\,\forall\,\mathbf{k},\,\forall\,m\in\mathcal{N}\setminus\tilde{m}$) *is a sufficient condition for* ($A_{\mathbf{k}}=0\,\forall\,\mathbf{k}$), *then the same* $\langle\alpha\rangle$*'s will be zero also in the minimizing solution of the constrained problem.*

In the case of half-filling the following corollary now follows for the two important cases of antiferromagnetic and s-wave superconducting ordering.[38]

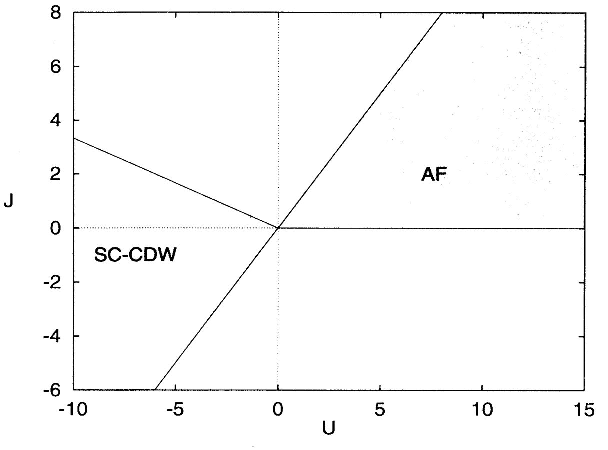

FIG. 2. The low energy states of the extended Hubbard model according to Corollary 1 is shown in grey. The white areas are indeterminate from the corollary, and the phases here must be computed numerically.

Corollary 1. *The state of lowest energy at half-filling* $(\mu = 0)$ *for the Hamiltonian* $(H = H_0+H_{\mathrm{Hubb}}+H_{\mathrm{Heis}})$ *in Eqs. (17), (18), and (19) is AF* $(\langle\alpha^2_{i0}\rangle \neq 0)$ *if* $0 < J < U$, *and s-wave SC-CDW* $(\langle\alpha^2_{0i}\rangle \neq 0)$ *if* $U < J < -U/3$.

The theorem follows by making two observations. First, the possible low-energy states follow from Theorem 1 by inspection of the prefactors of the quadratic terms in the Hamiltonian, and by verifying that $A_{\mathbf{k}} = 0$ if all $\langle\alpha\rangle$'s are zero except the hopping $\langle\alpha^1_{00}\rangle$ and either $\langle\alpha^2_{i0}\rangle$ or $\langle\alpha^2_{0i}\rangle$. Secondly, we observe that the problem that results by setting all other order parameters to zero is analogous to the ordinary s-wave SC case, where it is well known that any attractive interaction results in a finite order parameter.

We further note that there are two degenerate superconductivity solutions if the constraints are disregarded. One is the ordinary s-wave superconductor, and the other is the staggered superconductor. However, the latter is ruled out by the fact that the constraint $A_{\mathbf{k}} = 0$ is not fulfilled. Apart from predicting these low energy states, Theorem 1 also proves the stability of these phases with respect to small perturbations to the Hamiltonian. Since the ferromagnetic state has $A_{\mathbf{k}} \neq 0$, ferromagnetic ordering and nonzero hopping cannot be present simultaneously, at least not at the same location in $\mathbf{k}$ space. The predictions of the corollary are illustrated in Fig. 2.

It is interesting to compare our predictions with the model extended by the correlated hopping term in Eq. (6) with $X = t$ since there exists a rigorous criterion for when the SC state is the ground state of that model.[23] According to that criterion the system is superconducting when $-8|t| > U < J < -U/3$, which for sufficiently small U coincides exactly with our boundaries.

VII. NUMERICAL METHODS

To find the phase at a (U, J, μ, T) point in a phase diagram, we choose an initial value of the pitch vector $\mathbf{q}$, solve the self-consistent equations Eqs. (29), (30), and (32) numerically, and calculate $F(\mathbf{q})$ using Eqs. (34) and (35).

The pitch vector $\mathbf{q}$ is then varied to find which $\mathbf{q}$ gives the solution to the self-consistent equations with the lowest value of $F(\mathbf{q})$. The nonzero mean-field order parameters $\Delta_{l,m}$ defines, together with $\mathbf{q}$, the particular phase for the (U, J, μ, T) point in parameter space.

Complete phase diagrams are obtained by the following two steps.

The parameters $(U, J, \mu, T, \mathbf{q})$ are swept, with an initial set of Δ_m's generated at random and the self-consistent equations are iterated until a fixed point is reached. This gives us a rough picture of the states that are present in the phase diagram.

The accuracy of the boundaries between the phases in the phase diagram is improved. Here the self-consistent equations are solved using Broyden's method,[39] which is often more efficient than the previous iterative method.

To find $\Delta_{l,m}$ for a particular value of $\mathbf{q}$, we cover the reduced Brillouin zone by a discrete lattice. Care has to be taken not to break any of the symmetries of the problem. Figure 1 shows how a 32-point lattice is laid out. The most time-consuming numerical step is to diagonalize the 8×8 matrix in the argument of the exponential function in Eq. (32) at every $\mathbf{k}$ point; this must be done for each iteration.

Choosing random order parameters as initial conditions for recursion is useful when there is no *a priori* information about the expected solutions of the self-consistent equations. A complication of this method, however, is that the iteration tends to fall into cycles. We cured this by including a tail of exponentially damped previous iterates at each step. Sometimes, the procedure still did not converge, and several initial points must be used before a fixed point was found.

To obtain a complete μ-T phase diagram for fixed U and J, we cover the $(\mu, T, \mathbf{q})$ space with roughly 1500 points, and repeat the iterative procedure 10 times. On an ordinary workstation it takes of the order of a week of CPU time to trace out the phase diagram using 98 points in the reduced Brillouin zone and solving the self-consistent equations to an accuracy of 1%. Of course, solutions could be missed by chance since we use random initial guesses, and phases occurring in narrow regions of the phase space could be missed since the parameter space is not covered with a fine enough mesh.

After the different phases have been identified, we obtain more accurate solutions of the self-consistent equations using Broyden's method. This method cannot be used from the beginning since the initial guess has to be close to the final answer for the method to converge. The method is also slow if the number of order parameters is very large. Here, we therefore eliminate from the Hamiltonian all order parameters that are known to be zero in the corresponding regions.

If the state of lowest free energy has $\mathbf{q} = 0$ the minimizing solution can be obtained directly by Broyden's method, and in this case the phase boundaries are located to high accuracy, generally by using 800 points in the reduced Brillouin zone.

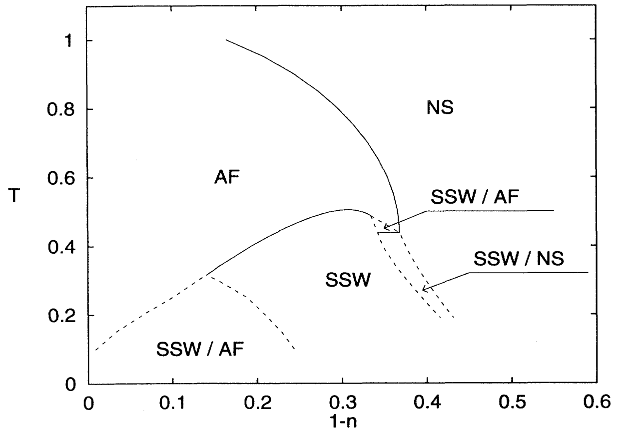

FIG. 7. Phase diagram for $U = 5$, $J = 0.1$. The SSW has pitch $(\pi - q, \pi)$.

pitch $(\pi - q, \pi)$, which is obtained by applying the twist $\mathbf{q} = (1,0)q$ to the AF (π,π) state. At low temperature, the SSW state is separated from the AF state by a first-order phase transition with a wide coexistence region as a function of density. For more elevated temperatures, the separation line becomes second-order and here the spiral pitch parameter q goes to zero as the phase boundary is approached. On the contrary, along the phase transition from the SSW to the normal state the spiral magnetic order parameter vanishes in magnitude while q stays finite. No superconductivity is seen in Fig. 6. The s-wave superconducting state is suppressed by the large value of U, and the d-wave state is not seen either since J is zero.

The energy gain of the spiral spin waves is numerically very small, of the order of a hundredth of the overall condensation energy. The introduction of a Heisenberg interaction could therefore have a large influence. To investigate this issue, we introduce a small $J = 0.1$ while keeping $U = 5$, and compare Fig. 6 with Fig. 7. What was a second order transition between the SSW and the normal state for $J = 0$ has now become first order. There is also a temperature range at which the AF is "reentrant" as a function of doping, and where the AF-SSW phase boundary move toward lower temperatures and becomes first order. When increasing J, this line of phase transitions rapidly migrate towards lower doping and very soon the whole spiral spin-wave region is gone. This explains why no spiral spin wave is seen in the phase diagrams for small U and large J.

For positive J and sufficiently low densities, the antiferromagnet and the spiral spin wave must eventually disappear, leaving room for the s-wave and d-wave superconducting states which may persist the rest of the way to zero filling. The critical temperature decreases rapidly with decreasing J and we were unable to confirm this scenario numerically.

IX. DISCUSSION

The Hubbard model serves as a simple model for high-T_c superconductors. Despite its simple appearance, the model is still poorly understood and many sophisticated techniques for studying specific features of the model have been proposed in the literature. As a guide to this realm of possibilities, it is important to have a good understanding of all possibilities that a "simple" mean-field analysis can provide. We have therefore used a generalized Hartree-Fock-Bogoliubov theory and numerical simulations to compute phase diagrams for the extended Hubbard model. All the conventional order parameters, like s- and d-wave superconductivity, charge-density waves, and Néel and spiral antiferromagnetic states, have been included in one unifying framework, making no *a priori* assumptions about the nature of the broken symmetries. We have further shown that, in mean-field theory, no new mixed phases arise at finite doping and temperature in the extended Hubbard model with positive values of U and J. In our investigation, we have seen the time-reversal symmetry-breaking superconducting phase $s + id$ only in a narrow region with negative U. Close to this region there is also a region of mixed antiferromagnetism and d-wave superconductivity. To place our approach in a still more general context, the mean-field method has been referred to as bosonic linearization since the Hamiltonian is expressed in terms of bosonic operators and is then linearized. Alternatively odd numbers of electron operators can be used to form new operators; the method is then called fermionic linearization.[37,41] This leads to a different dynamical group which has not yet been studied for the model we study here.

Our method allow phase separation to occur, which it also does in certain regions. The energy differences that we find between Néel and spiral antiferromagnets is so small, that we do not want to make any strong statements about whether phase coexistence would survive a more refined analysis or not. However, the energy difference between the AF and the normal state at the first order phase boundary is substantial. A phase separation between these two states has also been suggested both from theoretical and experimental grounds.[42] Another thing to keep in mind is that we require the total number of electrons to be fixed, while in the high-T_c materials there are large charge reservoirs surrounding the 2D planes that are perhaps better modeled by a fixed chemical potential. Under such circumstances, the phase coexistence may well be suppressed.

There have been several earlier studies of spiral spin waves for the Hubbard model exploiting slave-boson and ordinary Hartree-Fock techniques. Most of these studies have concentrated on zero temperature, and our corresponding results are consistent with those. However, we have also extended the analysis to finite temperature.

We have concentrated on a particular extension of the Hubbard model which preserves the pseudo-spin symmetry, and we have explored the phase diagrams in many parameter regimes. However, there are very few cases where we can compare our results with the ones obtained by other extensions of the Hubbard model, like nearest-neighbor Coulomb interaction and density-dependent hopping amplitudes. The application of our method to these other cases would thus be of great interest.

Another phenomenon that we have studied is how the spiral spin waves are affected by a nearest-neighbor Heisenberg term in the Hamiltonian. We have observed that the $(1,0)$ spiral spin-wave phase is easily destroyed upon the introduction of a positive-J Heisenberg interaction. We have mostly concentrated on spin waves in the $(1,0)$ direction since we found that the energy differences are very insensitive to the pitch direction, at least for the pure Hubbard model. To make the study complete, other spin directions should also be studied. However, it is likely that these small energy differences are insignificant with respect to the overall crudeness of our analysis, although one might argue that their relative difference is to be taken seriously.

ACKNOWLEDGMENT

The authors thank the Swedish Natural Research Council (NFR) for supporting this work.

APPENDIX A: THE POINT GROUP C_{4v}

The point-group symmetry of the 2D square lattice is C_{4v}, since the lattice is invariant under 90° rotations around the z axes and under reflections in the lines v and v' in Fig. 8. The group elements of C_{4v} are the identity (I), 90° rotations (C_4), 180° rotations (C_4^2), reflections in v (σ_v) and reflections in v' ($\sigma_{v'}$). This group has four 1D irreps (A_1, A_2, B_1, B_2) and one 2D irrep E. The character table together with examples of basis functions for the different irreps are given in Table II. Our main use of the C_{4v} irreps is to distinguish between d- and s-wave superconductivity order parameters. The s-wave ordering has the full symmetry of the lattice, i.e., it belongs to the A_1 representation. The d-wave ordering, on the other hand, is antisymmetric under reflections in v', and belongs to the B_1 representation. If we would see any p-wave states, these would belong to the 2D E representation since these states are antisymmetric under parity $[(x,y) \to (-x,-y)]$.

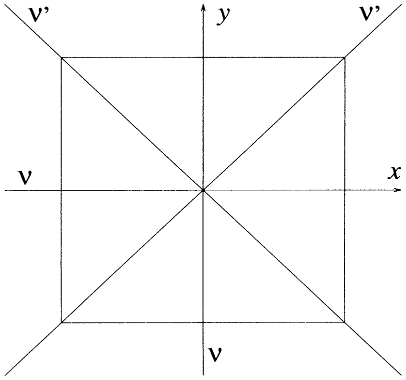

FIG. 8. The symmetry axes v and v' of the square lattice.

TABLE II. The character table of the point group C_{4v} together with examples of basis functions for the different irreducible representations.

	I	C_4^2	C_4	σ_v	$\sigma_{v'}$	Examples of functions
A_1	1	1	1	1	1	$1, \cos k_x + \cos k_y$
A_2	1	1	1	-1	-1	$\sin 2k_x \sin k_y - \sin 2k_y \sin k_x$
B_1	1	1	-1	1	-1	$\cos k_x - \cos k_y$
B_2	1	1	-1	-1	1	$\sin k_x \sin k_y$
E	2	-2	0	0	0	$\{\sin k_x, \sin k_y\}$

APPENDIX B: PROOFS OF THE ZERO-TEMPERATURE, HALF-FILLING THEOREMS

In this appendix we give the proofs of the theorems concerning the minimization of the ground-state energy. A bunch of related theorems have also been derived by Bach *et al.*[43] First we prove the lemma for how the energy minimization problem can be recast into the problem of minimizing the expectation value of the Hamiltonian written in terms of $\langle \alpha_{\mathbf{k}}^m \rangle$.

Lemma 1. *The restrictions on the expectation values* $\langle \alpha_{\mathbf{k}}^m \rangle$ *for the variational solutions of Eq. (20) are* $\sum_m \langle \alpha_{\mathbf{k}}^m \rangle^2 = \frac{1}{2}$, $\langle (\alpha_{00}^0)_{\mathbf{k}} \rangle = -\frac{1}{2}$, *and* $A_{\mathbf{k}} = 0 \; \forall \; \mathbf{k}$.

Proof. The space of all possible variational solutions is defined by the constraint that the Hermitian matrix $\langle G | \Psi_{\mathbf{k}}^\dagger \otimes \Psi_{\mathbf{k}} | G \rangle$ has the four-fold degenerate eigenvalues 0 and 1, since it has the same eigenvalues as $g = \langle G | (\chi_{\mathbf{k}}^\dagger \otimes \chi_{\mathbf{k}}) | G \rangle$. Our aim is to find the corresponding constraints on the coefficients $\langle \alpha_{\mathbf{k}}^m \rangle$ in the expansion

$$\langle G | \Psi_{\mathbf{k}}^\dagger \otimes \Psi_{\mathbf{k}} | G \rangle = \sum_m \langle \alpha_{\mathbf{k}}^m \rangle B_m \,. \tag{B1}$$

First of all, since $B_0 \equiv B_{00}^0 = -\mathbb{1}$ is the only basis matrix with a nonzero trace, one has $\langle (\alpha_{00}^0)_{\mathbf{k}} \rangle = -\frac{1}{2}$. Let us next define the traceless matrix $X_{\mathbf{k}}$,

$$X_{\mathbf{k}} \equiv \langle G | \Psi_{\mathbf{k}}^\dagger \otimes \Psi_{\mathbf{k}} | G \rangle - \tfrac{1}{2}\mathbb{1} \,. \tag{B2}$$

This matrix has the fourfold degenerate eigenvalues $\pm\frac{1}{2}$ and the expansion

$$X_{\mathbf{k}} = \sum_{m \neq 0} \langle \alpha_{\mathbf{k}}^m \rangle B_m \,. \tag{B3}$$

Furthermore, $\{X_{\mathbf{k}}, X_{\mathbf{k}}\}$ has the eightfold degenerate eigenvalue $\frac{1}{2}$, meaning that $\{X_{\mathbf{k}}, X_{\mathbf{k}}\} = \frac{1}{2}\mathbb{1}$, so that using Eq. (10) we have

$$\tfrac{1}{2}\mathbb{1} = \{X_{\mathbf{k}}, X_{\mathbf{k}}\} = \sum_{m \neq 0} 2\langle \alpha_{\mathbf{k}}^m \rangle^2 \mathbb{1} + A_{\mathbf{k}} \,, \tag{B4}$$

where $A_{\mathbf{k}}$ is the nondiagonal part defined in Eq. (37).

[26] S. C. Zhang, Phys. Rev. Lett. **65**, 120 (1990).

[27] S. C. Zhang, Int. J. Mod. Phys. B **5**, 153 (1991).

[28] S. C. Zhang, Phys. Rev. B **42**, 1012 (1990).

[29] S. Östlund and G. Mele, Phys. Rev. B **44**, 12 413 (1991).

[30] S. Östlund, Phys. Rev. Lett. **69**, 1695 (1992).

[31] J. B. Marston and I. Affleck, Phys. Rev. B **39**, 11 538 (1989).

[32] H. Shiba, Prog. Theor. Phys. **48**, 2171 (1972); V. J. Emery, Phys. Rev. B **14**, 2989 (1976).

[33] E. Fradkin, *Field Theories of Condensed Matter Systems* (Addison-Wesley, Redwood City, CA, 1991).

[34] E. H. Lieb and F. Y. Wu, Phys. Rev. Lett. **20**, 1445 (1968).

[35] W. Miller, Jr., *Symmetry Groups and their Applications* (Academic, New York, 1972).

[36] See, for example, J. W. Negele and H. Orland, *Quantum Many-Particle Systems* (Addison-Wesley, Redwood City, CA, 1988).

[37] A. Montorsi, M. Rasetti, and A. I. Solomon, Phys. Rev. Lett. **59**, 2243 (1987).

[38] We observe that the states in the corollary are exactly the states termed "unitary states" by A. I. Solomon and J. L. Birman, Phys. Lett. A **111**, 423 (1985).

[39] W. H. Press, S. A. Teukolsky, W. T. Vetterling, and B. P. Flannery, *Numerical Recipes in Fortran*, 2nd ed. (Cambridge University Press, Cambridge, England, 1992).

[40] R. Strack and D. Vollhardt, Phys. Rev. Lett. **72**, 3425 (1994).

[41] A. Danani, M. Rasetti, and A. I. Solomon, in *Theories of Matter*, edited by A. Solomon (World Scientific, Singapore, 1994).

[42] V. J. Emery and S. A. Kivelson, Physica C **209**, 597 (1993), and references therein.

[43] V. Bach, E. H. Lieb, and J. P. Solovej, J. Stat. Phys. **76**, 3 (1994).

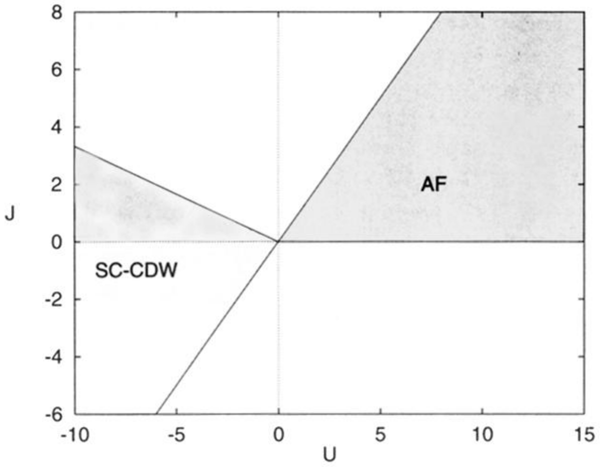

FIG. 2. The low energy states of the extended Hubbard model according to Corollary 1 is shown in grey. The white areas are indeterminate from the corollary, and the phases here must be computed numerically.